ASME Journal of Applied Mechanics
Online journal at:
https://asmedigitalcollection.asme.org/appliedmechanics

Thermomechanical Coupling in Polydomain Liquid Crystal Elastomers

Zhengxuan Wei[1]
Department of Mechanical and Industrial Engineering, College of Engineering, Northeastern University, Boston, MA 02115
e-mail: wei.zheng@northeastern.edu

Peixun Wang[1]
Department of Mechanical and Industrial Engineering, College of Engineering, Northeastern University, Boston, MA 02115
e-mail: wang.peix@northeastern.edu

Ruobing Bai[2]
Department of Mechanical and Industrial Engineering, College of Engineering, Northeastern University, Boston, MA 02115
e-mail: ru.bai@northeastern.edu

Liquid crystal elastomers (LCEs) are made of liquid crystal molecules integrated with rubber-like polymer networks. An LCE exhibits both the thermotropic property of liquid crystals and the large deformation of elastomers. It can be monodomain or polydomain in the nematic phase and transforms to an isotropic phase at elevated temperature. These features have enabled various new applications of LCEs in robotics and other fields. However, despite substantial research and development in recent years, thermomechanical coupling in polydomain LCEs remains poorly studied, such as their temperature-dependent mechanical response and stretch-influenced isotropic-nematic phase transition. This knowledge gap severely limits the fundamental understanding of the structure-property relationship, as well as future developments of LCEs with precisely controlled material behaviors. Here, we construct a theoretical model to investigate the thermomechanical coupling in polydomain LCEs. The model includes a quasi-convex elastic energy of the polymer network and a free energy of mesogens. We study the working conditions where a polydomain LCE is subjected to various prescribed planar stretches and temperatures. The quasi-convex elastic energy enables a "mechanical phase diagram" that describes the macroscopic effective mechanical response of the material, and the free energy of mesogens governs their first-order nematic-isotropic phase transition. The evolution of the mechanical phase diagram and the order parameter with temperature is predicted and discussed. Unique temperature-dependent mechanical behaviors of the polydomain LCE that have never been reported before are shown in their stress-stretch curves. These results are hoped to motivate future fundamental studies and new applications of thermomechanical LCEs. [DOI: 10.1115/1.4063219]

Keywords: liquid crystal elastomers, polydomain, phase transformation, thermomechanical coupling

1 Introduction

Liquid crystal elastomers (LCEs) are soft active materials that combine the orientational order of liquid crystal molecules (mesogens) and the entropic elasticity of rubber-like polymer networks. This inherent coupling at the molecular level provides LCEs with intriguing mechanical responses such as soft elasticity [1], high energy dissipation [2], and programmable anisotropy [3], as well as stimuli-responsive large deformation induced by thermal [3,4], photothermal [5,6], and photochemical [7–9] processes. As a result, LCEs have enabled exciting new applications in mechanics, materials, and robotics. Examples include thermomechanical actuators [10,11], light motors [12], shape morphing structures [13,14], energy dissipaters [2,15], and biomedical devices [16]. Accompanying these new applications is the rapid development of theories for various mechanical responses of LCEs under different loading conditions and/or stimuli, including monotonic load [1], biaxial load [17,18], bending [19,20], heating [21], and light illumination [7,8].

In a typical thermotropic main-chain LCE, LC mesogens are linked in the linear polymer chains of a stretchable amorphous polymer network. The rod-like mesogens form a *nematic* phase with a long-range orientational order at low temperature (e.g., room temperature) and transform to an *isotropic* phase with no orientational order at temperature above a nematic-isotropic transition temperature (e.g., around 60 °C [22]). The low-temperature nematic phase can be either *monodomain* with a uniform mesogen orientation or *polydomain* with many co-existing domains of different mesogen orientations. These different phases and domain formations significantly affect the mechanical (stress-stretch) responses of their corresponding LCEs [23]. In brief, an isotropic LCE at high temperature has isotropic, common rubber-like mechanical responses, a nematic monodomain LCE has anisotropic mechanical responses due to the uniform mesogen order, and a nematic polydomain LCE has macroscopically isotropic mechanical responses due to the co-existing domains at the microscale.

This paper focuses on the elastic responses of nematic polydomain LCEs. Understanding the fundamental mechanics of polydomain LCEs is of great importance to their future research and development for two reasons. First, fundamentally, the mechanical

[1]These authors have contributed equally to this work.
[2]Corresponding author.

Contributed by the Applied Mechanics Division of ASME for publication in the Journal of Applied Mechanics. Manuscript received August 1, 2023; final manuscript received August 14, 2023; published online September 11, 2023. Tech. Editor: Pradeep Sharma.

behavior of polydomain LCEs can be considered as a more general case that involves the mesogen director rotation [1,24–26] during deformation, compared to behaviors of monodomain LCEs without involving such mesogen rotation. Second, in practice, a polydomain LCE is the immediate product of the first-step synthesis during the widely used two-step fabrication of LCEs in experiment [27], where the synthesized polydomain sample is subsequently stretched and crosslinked in the second step to form the final monodomain sample.

In studying the important physical parameters and processes in an LCE, temperature is the only parameter that critically affects both the nematic-isotropic phase transition of mesogens and the entropic elasticity of the polymer network. However, despite recent progresses in the theoretical modeling [1,24,25,28], numerical simulation [18], and experimentation [18,29] of polydomain LCEs, thermomechanical coupling in polydomain LCEs, such as the temperature-dependent mechanical response and the stretch-dependent isotropic-nematic phase transition, is not well studied. This knowledge gap severely limits the future development of LCEs with the aim of precisely controlling their behaviors under various temperatures and mechanical loads. This lack of knowledge further hinders the goal of establishing a quantitative relationship between material parameters and the final material property, to replace the current empirical approach in the fabrication of LCEs that involves temperature change and stretching of polydomain samples.

Here, we develop a theoretical model to study the thermomechanical coupling in polydomain LCEs. The continuum model includes a quasi-convex elastic energy of the polymer network and a free energy of mesogens (Sec. 2). Building on this model, we investigate working conditions where a polydomain LCE is subjected to various prescribed planar stretches and temperatures. The quasi-convex elastic energy enables a "mechanical phase diagram" that describes the macroscopic effective mechanical response of the material, and the free energy of mesogens governs the first-order nematic-isotropic phase transition (Sec. 3). Evolution of the mechanical phase diagram and the order parameter with temperature is predicted and discussed (Sec. 4). Unique temperature-dependent mechanical behaviors of the polydomain LCE that have never been reported before are shown in their stress-stretch curves (Sec. 5).

2 Theoretical Model

The general theoretical framework is illustrated in Fig. 1. Throughout this paper, we use T_{ni} to represent the nematic-isotropic phase transition temperature of mesogens without any additional coupling from mechanical stretch. The high-temperature isotropic phase at $T > T_{ni}$ is chosen as the reference state (Fig. 1(*a*)). At a temperature $T < T_{ni}$ without any mechanical stretch, the LCE stays in the nematic phase with polydomain, where different domains have different mesogen orientations (Fig. 1(*b*)). In the current state, the LCE is subjected to planar tensile stretches λ_2 and λ_3, with the corresponding true stresses s_2 and s_3 (Fig. 1(*c*)). For mathematical convenience, the principal stretches satisfy $\lambda_3 \geq \lambda_2 \geq \lambda_1$ [25,28]. We will investigate various temperatures both below and above T_{ni} in the current state.

Following DeSimone et al. [25,26,28], we adopt a quasi-convex elastic energy for the LCE polymer network as

$$W_{qc}(\lambda_i, Q) = \begin{cases} \dfrac{NkT}{2}\left(\dfrac{3a^{1/3}}{1-Q} + [\log(1+2Q)(1-Q)^2]\right) & \text{Phase L, } \lambda_1 \geq a^{1/6} \\ \dfrac{NkT}{2}\dfrac{1}{1-Q}(\lambda_1^2 + \lambda_2^2 + a\lambda_3^2 + [\log(1+2Q)(1-Q)^2]) & \text{Phase S, } a^{1/2}\lambda_3^2\lambda_1 > 1 \\ \dfrac{NkT}{2}\dfrac{1}{1-Q}(\lambda_1^2 + 2a^{1/2}\lambda_1^{-1} + [\log(1+2Q)(1-Q)^2]) & \text{Phase Sm, else} \end{cases} \quad (1)$$

where Q is the nematic order parameter ($Q = 0$ represents the isotropic phase without directional order of mesogens, $Q = 1$ represents perfect alignment of mesogens, and $0 < Q < 1$ represents the general nematic phase), $a = (1-Q)/(1+2Q)$, N is the number of polymer chains per unit volume, kT is the temperature in the unit of energy, and NkT is the shear modulus of the elastomer. The three phases "L," "S," and "Sm" correspond to different macroscopic mechanical behaviors of the polydomain LCE, which will be discussed in Sec. 3.1. Here we further modify the form of the free energy to make it consistent with the original form derived

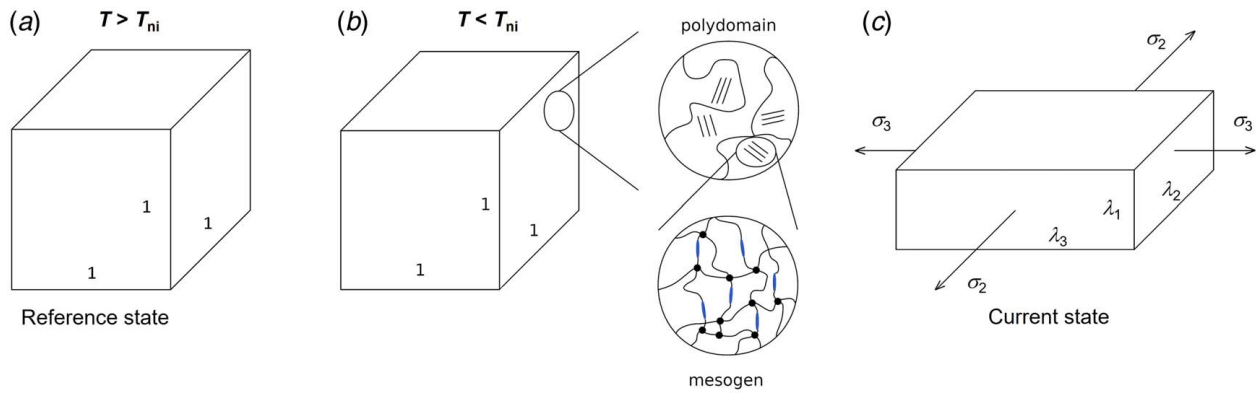

Fig. 1 Theoretical framework of a polydomain LCE subjected to various prescribed planar stretches and temperatures. T_{ni} is the nematic-isotropic phase transition temperature of mesogens without any additional coupling from mechanical stretch: (*a*) the high-temperature isotropic phase at $T > T_{ni}$ is chosen as the reference state, (*b*) the microstructure of a polydomain LCE at a temperature $T < T_{ni}$, and (c) in the current state, the LCE is subjected to planar tensile stretches λ_2 and λ_3, with the corresponding true stresses s_2 and s_3. The principal stretches satisfy $\lambda_3 \geq \lambda_2 \geq \lambda_1$. We will investigate various temperatures both below and above T_{ni} in the current state.

by Bladon et al. for monodomain LCEs [23,30], to ensure the accurate terms containing Q in the model, which will affect the thermo-mechanical coupling to be investigated later.

The continuum model also includes the Maier–Saupe free energy that describes the long-range dipolar interaction between mesogens in the LCE [31–33], expressed as

$$W_{\mathrm{lc}}(Q) = N_{\mathrm{n}} kT\left[g^{-1}(Q)Q - \log Z(Q) - \frac{J}{2kT}Q^2\right] \tag{2}$$

where

$$g(x) = -\frac{1}{2} - \frac{1}{2x} + \frac{1}{2x}\sqrt{\frac{3x}{2}}\frac{\exp(3x/2)}{\int_0^{\sqrt{3x/2}}\exp(y^2)dy} \tag{3}$$

$$Z(Q) = \frac{\exp[g^{-1}(Q)]}{1 + g^{-1}(Q)(1+2Q)} \tag{4}$$

N_{n} is the number of mesogens per unit volume, and J is the interaction parameter between mesogens in the unit of energy.

The total free energy of the system is expressed as

$$W(\lambda_i, Q) = W_{\mathrm{qc}}(\lambda_i, Q) + W_{\mathrm{lc}}(Q) \tag{5}$$

By assuming the incompressibility of the elastomer, we have $\lambda_1\lambda_2\lambda_3 = 1$. Using this to express the out-of-plane stretch $\lambda_1 = 1/\lambda_2\lambda_3$, in thermodynamic equilibrium, we have

$$\frac{\partial W(\lambda_2, \lambda_3, Q)}{\partial Q} = 0 \tag{6}$$

Table 1 Dimensionless groups in the model

Dimensionless group	Expression	Numerical value
Average interaction parameter between mesogens	$\hat{J} = J/kT_{\mathrm{ni}}$	4.54
Number of polymer chains per unit volume of the elastomer	$\hat{N} = N/N_{\mathrm{n}}$	0.05
Temperature	$\hat{T} = T/T_{\mathrm{ni}}$	Varying
True stress	$\hat{\sigma}_i = \sigma_i/NkT_{\mathrm{ni}}$	Varying
Free energy	$\hat{W} = W/N_{\mathrm{n}}kT_{\mathrm{ni}}$	Varying

$$\begin{cases} \sigma_2 = \lambda_2 \dfrac{\partial W(\lambda_2, \lambda_3, Q)}{\partial \lambda_2} \\ \sigma_3 = \lambda_3 \dfrac{\partial W(\lambda_2, \lambda_3, Q)}{\partial \lambda_3} \end{cases} \tag{7}$$

where s_2 and s_3 are the principal true stresses in the planar directions and $s_1 = 0$. Substituting Eqs. (1) and (5) into Eq. (7), we obtain the specific forms of s_2 and s_3 as

$$\begin{cases} \sigma_2 = \sigma_3 = 0 & \text{Phase L, } \lambda_1 \geq a^{1/6} \\ \sigma_2 = \dfrac{NkT}{1-Q}\left[\lambda_2^2 - \dfrac{1}{(\lambda_2\lambda_3)^2}\right] & \text{Phase S, } a^{1/2}\lambda_3^2\lambda_1 > 1 \\ \sigma_3 = \dfrac{NkT}{1-Q}\left[a\lambda_3^2 - \dfrac{1}{(\lambda_2\lambda_3)^2}\right] & \text{Phase S, } a^{1/2}\lambda_3^2\lambda_1 > 1 \\ \sigma_2 = \sigma_3 = \dfrac{NkT}{1-Q}\left[a^{\frac{1}{2}}\lambda_2\lambda_3 - \dfrac{1}{(\lambda_2\lambda_3)^2}\right] & \text{Phase Sm, else} \end{cases} \tag{8}$$

Finally, we introduce the following dimensionless groups in Table 1. In particular, we choose the dimensionless interaction parameter $\hat{J} = 4.54$ such that the nematic-isotropic transition takes place at $\hat{T} = T/T_{\mathrm{ni}} = 1$ when no effect of mechanical stretch is considered [8,33] (to be discussed in Sec. 3.2).

3 Uncoupled Mechanical and Thermal Behaviors

3.1 Macroscopic Effective Mechanical Responses. We first construct a mechanical phase diagram to describe the macroscopic effective mechanical response of a polydomain LCE under different planar stretches, based on the area stretch ratio $1/\lambda_1 = \lambda_2\lambda_3$ and the largest principal stretch l_3 (Fig. 2(*a*)). To do so, we fix the temperature at $\hat{T} = 0.8$ and use Eqs. (1)–(6) to solve for Q through finding the global minimum of the total free energy $W(\lambda_i, Q)$ at different stretch values (the distributed values of Q in the phase diagram will be discussed in Figs. 3 and 4). Afterward, we identify the external and internal boundaries of the phase diagram following the original work of DeSimone et al. [25,26,28].

The phase diagram is bounded by two external boundaries, $1/\lambda_1 \geq \sqrt{\lambda_3}$ and $1/\lambda_1 \leq \lambda_3^2$, corresponding to the uniaxial and equal-biaxial loading paths, respectively. This is a result of incompressibility $\lambda_1\lambda_2\lambda_3 = 1$ and $\lambda_3 \geq \lambda_2 \geq \lambda_1$ in the model setup. In addition, the phase diagram consists of three "mechanical phases," as discussed in the following.

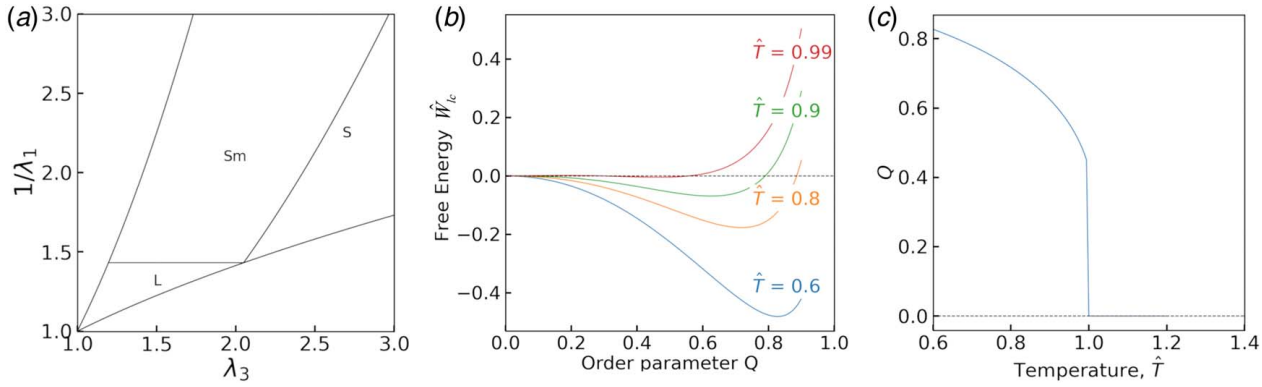

Fig. 2 (*a*) Mechanical phase diagram describes the macroscopic effective mechanical response of a polydomain LCE under different planar stretches. The dimensionless temperature is fixed as $\hat{T} = 0.8$, (*b*) the normalized Maier–Saupe free energy as a function of order parameter Q at different dimensionless temperatures $\hat{T} = 0.6, 0.8, 0.9, 0.99$. The free energy evolves from a single-well structure at low temperature to a double-well structure at temperature close to $\hat{T} = 1$, indicating the first-order nematic-isotropic phase transition. A small but positive energy barrier exists between the two wells, which is hardly seen in the plot but is confirmed by the simulation; and (*c*) the equilibrium order parameter Q at different temperatures considers only the Maier–Saupe free energy. The first-order nematic-isotropic phase transition is indicated by the discontinuity of the curve at $\hat{T} = 1$.

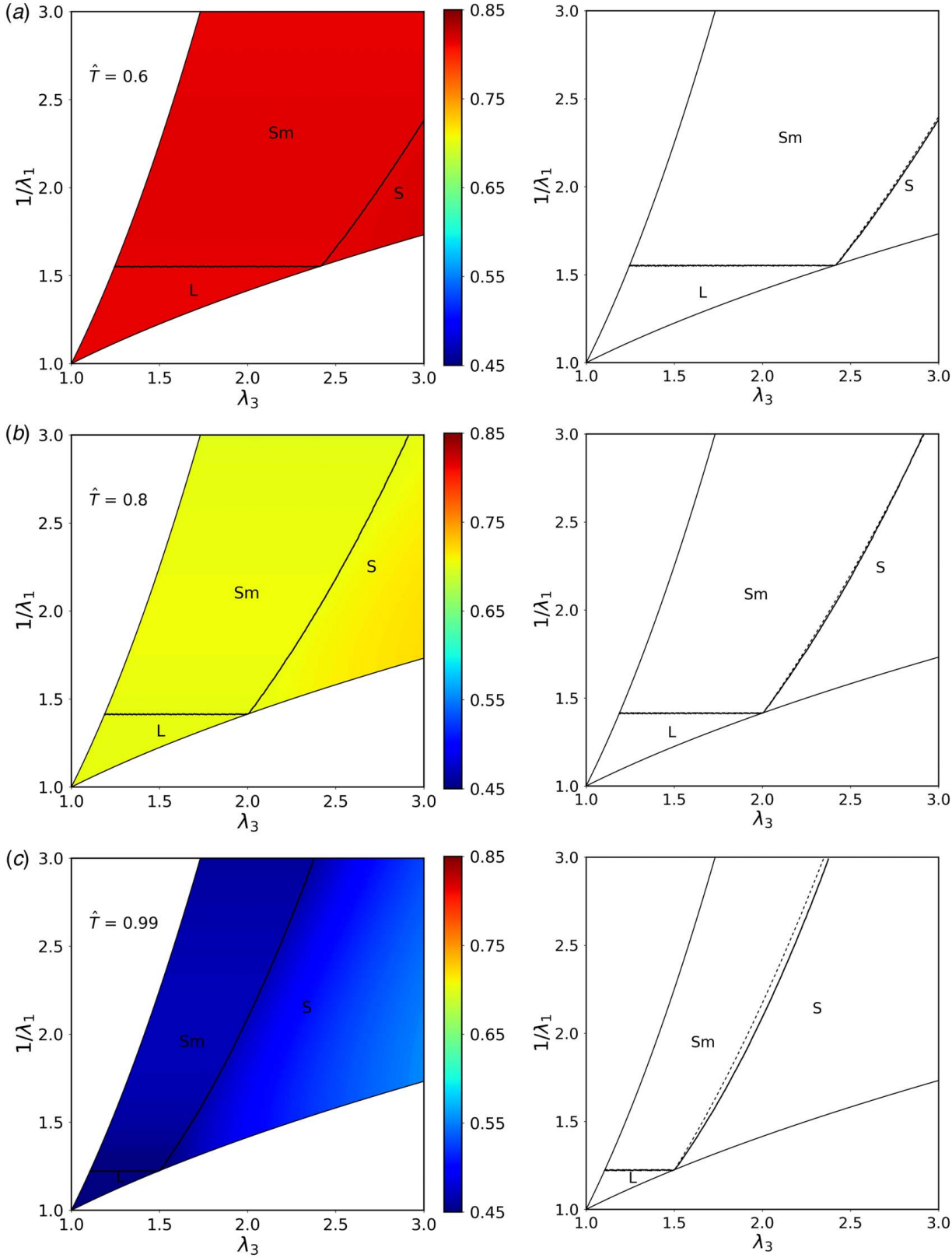

Fig. 3 Mechanical phase diagrams at temperatures below T_{ni} with distributions of the equilibrium order parameter Q: (*a*) $\hat{T} = 0.6$, (*b*) $\hat{T} = 0.8$, and (*c*) $\hat{T} = 0.99$. The right column shows the phase boundaries only. Solid lines are calculated using both free energies, and dashed lines are calculated using only the Maier–Saupe free energy.

In *Phase L* (liquid), the solid-state polydomain LCE behaves liquid-like—the material shows zero stress despite finite principal stretches. This is a direct consequence of the infinite ground states of the quasi-convex elastic energy, stemming from the coupling between mesogen rotation and polymer chain stretching during deformation. This phenomenon of zero stress with finite stretches is called *soft elasticity*, which has been widely reported in LCEs before [23,24].

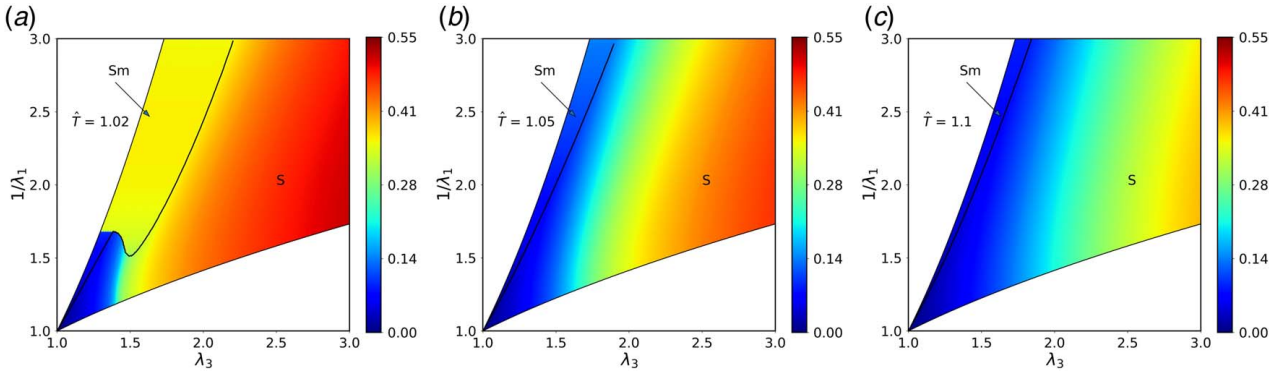

Fig. 4 Mechanical phase diagrams at temperatures above T_{ni} with distributions of the equilibrium order parameter Q: (*a*) $\hat{T} = 1.02$, (*b*) $\hat{T} = 1.05$, and (*c*) $\hat{T} = 1.1$

In *Phase Sm* (smectic) upon further biaxial stretches, the polydomain LCE behaves solid-like when being stretched out of plane (along l_1) but behaves liquid-like when being stretched in plane. The free energy in Phase Sm only depends on the out-of-plane stretch l_1, such that the LCE always shows identical biaxial true stresses s_2 and s_3 in this mechanical phase (Eq. (8)). This phenomenon has been recently validated in experiment and analyzed in numerical simulation [18].

Further biaxial or uniaxial stretches also lead to *Phase S* (solid), where the LCE behaves like a common rubber. In particular, under the uniaxial stretch state in Phase S, the LCE transforms to monodomain, with all the mesogens aligned along the uniaxial stretch direction l_3 [23].

The boundary between Phase L and Phase Sm is described by $1/\lambda_1 = a^{-1/6}$ with $a^{-1/3} \le \lambda_3 \le a^{-1/12}$, and the boundary between Phase Sm and Phase S is described by $1/\lambda_1 = a^{1/2}\lambda_3^2$ [25,26,28], where $a = (1-Q)/(1+2Q)$. As a result, the mechanical phase diagram is temperature-dependent, through the thermal-induced change of the order parameter Q, as discussed next.

3.2 Nematic-Isotropic Phase Transition. To illustrate the dominant effect of temperature on the order parameter Q and the corresponding thermal-induced nematic-isotropic phase transition, we first only consider the Maier–Saupe free energy. This represents a system of only liquid crystal mesogens without any polymer network. The energy landscape as a function of Q at various temperatures shows a first-order phase transition (Fig. 2(*b*)). For temperatures much below the nematic-isotropic transition temperature T_{ni} (e.g., $\hat{T} = 0.6$, 0.8, and 0.9), the Maier–Saupe free energy has a single-well structure where the free energy is minimized at Q between 0 and 1, representing the nematic phase. When the temperature approaches T_{ni}, or $\hat{T}$ approaches 1, the free energy transforms to a double-well structure with a second minimum at $Q = 0$ in addition to the minimum at a finite Q, together with a small but positive energy barrier between the two minima (hardly seen in the plot but confirmed by the simulation), indicating a weak first-order nematic-isotropic phase transition. This is also shown in Fig. 2(*c*) with the equilibrium order parameter Q as a function of temperature. The first-order nematic-isotropic phase transition is indicated by the discontinuity of the curve at $\hat{T} = 1$.

4 Thermomechanical Coupling

We next consider the general case of a system including both the quasi-convex elastic energy of the polymer network and the Maier–Saupe free energy of the mesogen mixture. As will be shown, both temperature and mechanical stretch will affect the mechanical phase boundaries and the corresponding stress-stretch responses.

4.1 Mechanical Phase Boundaries at Temperatures Below T_{ni}. Figure 3 illustrates the evolution of mechanical phase boundaries at temperatures below T_{ni}, as well as the color map of the equilibrium Q at different stretches. As temperature increases (e.g., $\hat{T} = 0.6$, 0.8, and 0.99, Figs. 3(*a*)–3(*c*)), the areas of Phase L and Phase Sm decrease while the area of Phase S increases, indicating a more pronounced common rubber-like behavior of the LCE. Furthermore, under the same stretch, the order parameter Q decreases with increasing temperature, consistent with the trend toward the nematic-isotropic transition shown in Figs. 2(*b*) and 2(*c*). The near-uniform color distribution of Q at different temperatures indicates its weak dependence on stretch at temperatures below T_{ni}. This confirms a long-time adopted assumption in the theory and simulation of LCEs, where the order parameter Q or the parameter $a = (1-Q)/(1+2Q)$ is almost always considered as a constant independent of deformation at a fixed temperature below T_{ni} [18,24,25,28].

To further show the effect of mechanical stretch on Q and phase boundaries, we also plot phase boundaries using the uncoupled equilibrium Q when considering only the Maier–Saupe free energy (Fig. 2(*c*)). The phase boundaries calculated using both free energies and using only the Maier–Saupe free energy are compared in Figs. 3(*a*)–3(*c*) right (solid and dashed lines, respectively). Indeed, a negligible difference is found, and the difference becomes larger with increasing temperature. By considering thermomechanical coupling (i.e., including both free energies), the phase boundary between Phases Sm and S shifts toward a higher l_3. Overall, at temperatures below T_{ni}, the thermal effect dominates the equilibrium order parameter Q.

4.2 Mechanical Phase Boundaries at Temperatures Above T_{ni}. The effect of mechanical stretch on Q is much more pronounced at temperatures above T_{ni}. Without considering thermomechanical coupling by calculating Q using only the Maier–Saupe free energy, we have $Q = 0$ and $a = 1$. In this case, all the phase boundaries degenerate to a single point of $l_1 = l_2 = l_3 = 1$, leaving only Phase S in the phase diagram. This represents a common rubber-like mechanical behavior. By contrast, with thermomechanical coupling by calculating Q using both free energies, an additional finite area of Phase Sm emerges even at temperatures above T_{ni} (Fig. 4). The area of Phase Sm decreases with increasing temperature. No Phase L is found at any temperature above T_{ni}.

This emergence of Phase Sm at temperature above T_{ni} is essentially due to the stretch effect on the equilibrium order parameter Q and the nematic-isotropic transition. As shown in Fig. 4, increasing the uniaxial stretch l_3 and area stretch $1/l_1$ significantly increases the equilibrium Q from nearly 0 to about 0.55. This large stretch-dependence of Q at $\hat{T} > 1$, which dramatically contrasts with the cases at $\hat{T} < 1$, indicates a possible stretch-induced transition of mesogens from the isotropic phase back to the nematic phase. Effectively, the non-zero uniaxial stretch l_3 or area stretch $1/l_1$ increases the nematic-isotropic transition temperature. This behavior is consistent with the previously reported stretch effect on

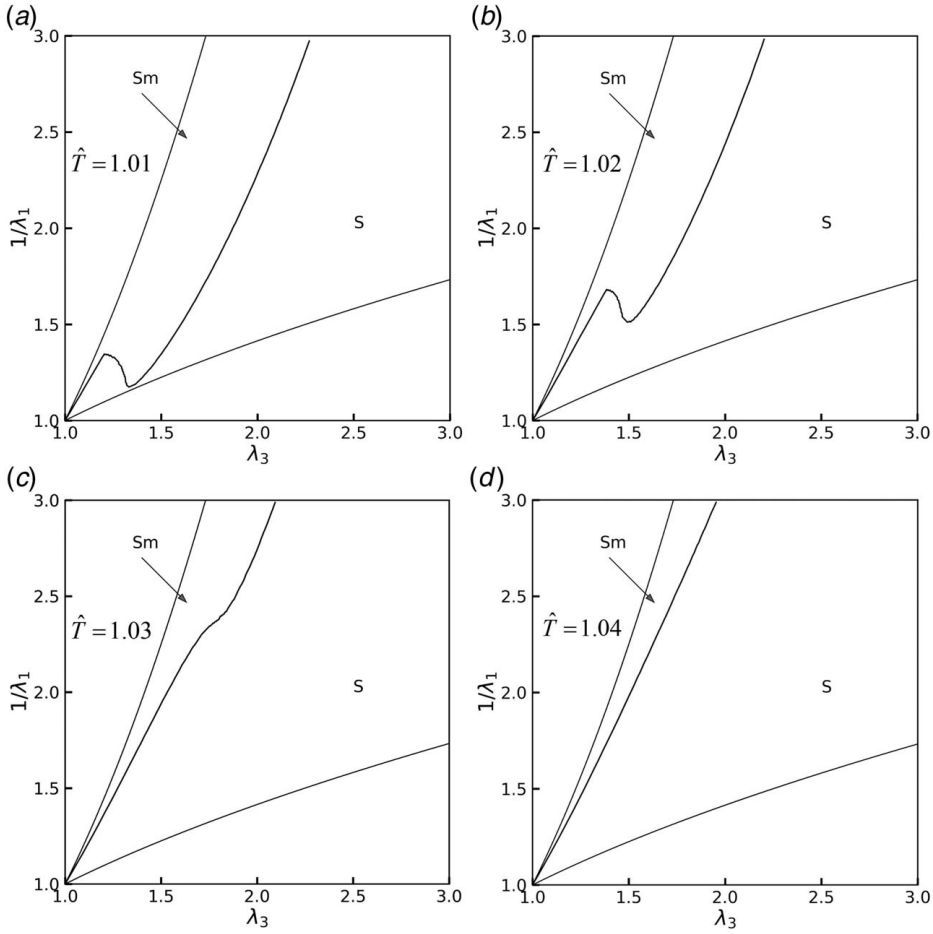

Fig. 5 Mechanical phase diagrams at temperatures slightly higher than T_{ni}: (*a*) $\hat{T}=1.01$, (*b*) $\hat{T}=1.02$, (c) $\hat{T}=1.03$, and (*d*) $\hat{T}=1.04$

the nematic-isotropic phase transition under the uniaxial mechanical load [7–9,34]. Finally, when the temperature is only slightly higher than T_{ni} (e.g., $\hat{T}=1.02$, Fig. 4(*a*)), the large stretch-dependence of Q leads to a "nose"-shaped phase boundary between Phases Sm and S.

To examine the evolution of phase boundaries more carefully at temperatures slightly higher than T_{ni}, we plot phase boundaries at $\hat{T}=1.01$, 1.02, 1.03, and 1.04 in Fig. 5. As the temperature increases, the phase boundary between Phases Sm and S transforms from a deep "nose" shape to a smooth line, with the area of Phase

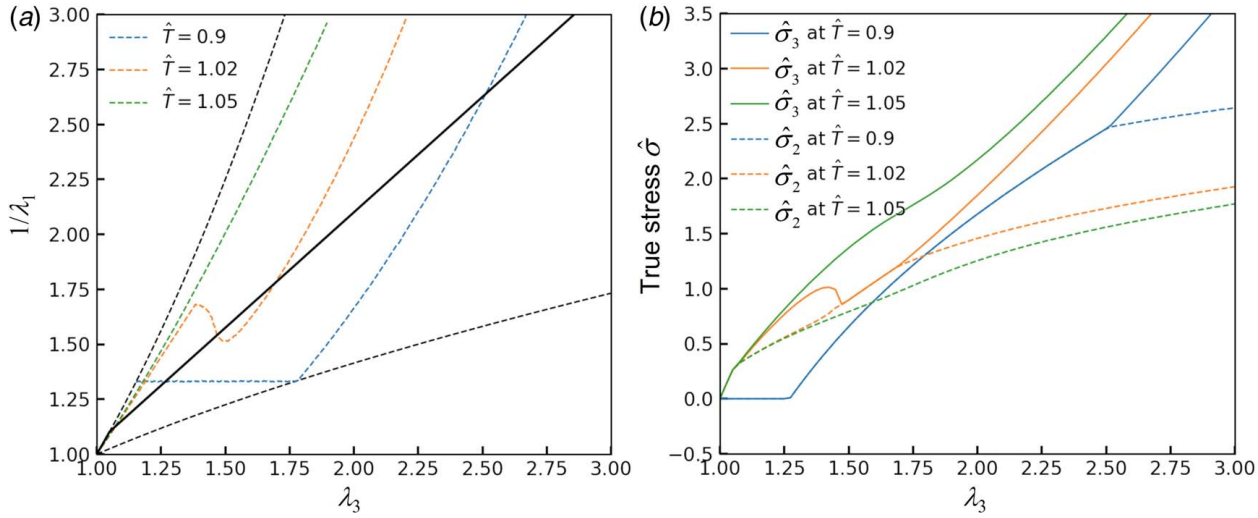

Fig. 6 (*a*) A specific loading path is indicated by the solid black line. A sheet of LCE is initially under equal-biaxial stretch up to $\lambda_2=\lambda_3=1.05$. Afterward, we fix $\lambda_2=1.05$ and only increase λ_3. The phase boundaries between Phases Sm and S at different temperatures are plotted as dashed lines, together with the two external boundaries defined by the uniaxial and equal-biaxial stretch states (dashed lines at the top and bottom). (*b*) The true stresses $\hat{\sigma}_2$ and $\hat{\sigma}_3$ as functions of I_3, under the specific loading path in (*a*) at different temperatures.

Sm decreasing. We conclude that the emergence of this "nose"-shaped phase boundary results from the three-way coupling between the temperature dependence of Q, the stretch dependence of Q, and the phase boundary governed by Q. To the best of our knowledge, this phenomenon has never been reported before. Our preliminary experiment of biaxial test at a fixed temperature seems to have qualitatively validated this theoretical prediction, and we are currently conducting a systematic experimental study on this unusual phenomenon.

5 Stresses-Stretch Responses

The evolution of mechanical phase boundaries due to thermomechanical coupling has a profound effect on the stress-stretch behavior of the polydomain LCE. To show this, we investigate a specific loading path defined by the biaxial stretches λ_2 and λ_3, as illustrated by the solid black line in Fig. 6(*a*). At a fixed temperature, a sheet of LCE is initially under equal-biaxial stretch up to $\lambda_2 = \lambda_3 = 1.05$. Afterward, we fix $\lambda_2 = 1.05$ and only increase λ_3. We study three distinct scenarios with temperatures of $\hat{T} = 0.9$, 1.02, and 1.05. The phase boundaries between Phases Sm and S are plotted as the dashed lines in Fig. 6(*a*). We calculate the planar true stresses $\hat{\sigma}_2$ and $\hat{\sigma}_3$ using Eq. (8) and plot them as functions of l_3 in Fig. 6(*b*).

In the first scenario at $\hat{T} = 0.9$, the loading path crosses all the three phases one by one through L, Sm, and S. Phase L exists in this case since the LCE is in the nematic phase ($\hat{T} < 1$). Both $\hat{\sigma}_2$ and $\hat{\sigma}_3$ are zero in Phase L, showing the soft elastic behavior [23]. Entering Phase Sm, $\hat{\sigma}_2$ and $\hat{\sigma}_3$ increase with l_3 while being always identical to each other, as illustrated by Eq. (8) and discussed in Sec. 3.1. Note that this is a non-equal-biaxial stretch state with $\lambda_2 = 1.05$ fixed and only λ_3 increased. In other words, in Phase Sm, the polydomain LCE can have non-zero planar shear strain (since $\lambda_2 \neq \lambda_3$) but can never have any planar shear stress (since $\hat{\sigma}_2 = \hat{\sigma}_3$ always holds). Finally, in Phase S, $\hat{\sigma}_2$ and $\hat{\sigma}_3$ deviate from each other and $\hat{\sigma}_3$ becomes larger, since the LCE sheet is stretched in the λ_3 direction with λ_2 fixed.

In the second scenario at $\hat{T} = 1.02$, there is no Phase L. The loading path starts with Phase S, transverses through Phase Sm, and reenters Phase S again. Recall that in general, $\hat{\sigma}_2 = \hat{\sigma}_3$ always holds in Phase Sm, and $\hat{\sigma}_3 > \hat{\sigma}_2$ holds in Phase S due to the specific loading path prescribed here. As a result, after the initial equal-biaxial stretch, $\hat{\sigma}_3$ first increases to be larger than $\hat{\sigma}_2$ in Phase S, drops back to be identical to $\hat{\sigma}_2$ in Phase Sm, and increases to be larger than $\hat{\sigma}_2$ again due to the reentrant transformation from Phase Sm to Phase S in the material.

In the third scenario at $\hat{T} = 1.05$, the loading path is almost entirely in Phase S, and the material behaves like a common rubber with $\hat{\sigma}_3 > \hat{\sigma}_2$.

We further note that while the stress-stretch responses of polydomain LCEs in the first and third scenarios have been well-understood based on previous studies, the second scenario that involves the reentrant transformation due to the "nose"-shaped phase boundary has never been reported before. This again shows the pronounced effect of mechanical stretch on the equilibrium Q in thermomechanical coupling at temperatures slightly above T_{ni}. Further experimental investigation of this phenomenon is currently under study.

6 Conclusion

In this paper, we have constructed a theoretical model to investigate thermomechanical coupling in polydomain LCEs subjected to various planar stretches and temperatures. The thermal-induced change of order parameter and the corresponding nematic-isotropic transition in the LCE greatly affect the mechanical phase boundaries as well as the macroscopic stress-stretch behaviors. On the other hand, mechanical stretch has a negligible effect on the equilibrium order parameter and mechanical phase boundaries at temperatures below the nematic-isotropic transition temperature T_{ni}, but has a significant effect at temperatures above T_{ni}. When the temperature is slightly higher than T_{ni}, thermomechanical coupling leads to the existence of Phase Sm as well as a unique "nose"-shaped phase boundary between Phases Sm and S. The corresponding stress-stretch response shows a non-monotonic behavior at certain loading paths of biaxial stretches. The planar true stresses are always zero in Phase L regardless of the stretch, and are always identical in Phase Sm, only depending on the out-of-plane stretch. The material behaves like a common elastic rubber in Phase S. We hope these theoretical findings can motivate further experiment and model developments on thermomechanical coupling in LCEs, as well as provide guidelines for future designs of complex actuation in LCE-based robots and structures. Effects of non-ideal polymer chains (additional coupling between polymer chains and mesogen directions at the state when the LCE is fabricated) and viscoelasticity on the behaviors reported in this paper deserve further systematic investigation.

Acknowledgment

This work was supported by the National Science Foundation through grant CMMI-2146409.

Conflict of Interest

There are no conflicts of interest.

Data Availability Statement

The datasets generated and supporting the findings of this article are obtainable from the corresponding author upon reasonable request.

References

[1] Biggins, J. S., Warner, M., and Bhattacharya, K., 2009, "Supersoft Elasticity in Polydomain Nematic Elastomers," Phys. Rev. Lett., **103**(3), p. 037802.
[2] Traugutt, N. A., Mistry, D., Luo, C., Yu, K., Ge, Q., and Yakacki, C. M., 2020, "Liquid-Crystal-Elastomer-Based Dissipative Structures by Digital Light Processing 3D Printing," Adv. Mater., **32**(28), p. 2000797.
[3] White, T. J., and Broer, D. J., 2015, "Programmable and Adaptive Mechanics With Liquid Crystal Polymer Networks and Elastomers," Nat. Mater., **14**(11), pp. 1087–1098.
[4] Guin, T., Settle, M. J., Kowalski, B. A., Auguste, A. D., Beblo, R. V., Reich, G. W., and White, T. J., 2018, "Layered Liquid Crystal Elastomer Actuators," Nat. Commun., **9**(1), p. 2531.
[5] Kuenstler, A. S., Chen, Y., Bui, P., Kim, H., DeSimone, A., Jin, L., and Hayward, R. C., 2020, "Blueprinting Photothermal Shape-Morphing of Liquid Crystal Elastomers," Adv. Mater., **32**(17), p. 2000609.
[6] Zhang, W., Nan, Y., Wu, Z., Shen, Y., and Luo, D., 2022, "Photothermal-Driven Liquid Crystal Elastomers: Materials, Alignment and Applications," Molecules, **27**(14), p. 4330.
[7] Bai, R., and Bhattacharya, K., 2020, "Photomechanical Coupling in Photoactive Nematic Elastomers," J. Mech. Phys. Solids, **144**, p. 104115.
[8] Wei, Z., and Bai, R., 2022, "Temperature-Modulated Photomechanical Actuation of Photoactive Liquid Crystal Elastomers," Extreme Mech. Lett., **51**, p. 101614.
[9] Finkelmann, H., Nishikawa, E., Pereira, G. G., and Warner, M., 2001, "A New Opto-Mechanical Effect in Solids," Phys. Rev. Lett., **87**(1), p. 015501.
[10] Merkel, D. R., Traugutt, N. A., Visvanathan, R., Yakacki, C. M., and Frick, C. P., 2018, "Thermomechanical Properties of Monodomain Nematic Main-Chain Liquid Crystal Elastomers," Soft Matter, **14**(29), pp. 6024–6036.
[11] Kularatne, R. S., Kim, H., Boothby, J. M., and Ware, T. H., 2017, "Liquid Crystal Elastomer Actuators: Synthesis, Alignment, and Applications," J. Polym. Sci., Part B: Polym. Phys., **55**(5), pp. 395–411.
[12] Yamada, M., Kondo, M., Mamiya, J.-I., Yu, Y., Kinoshita, M., Barrett, C. J., and Ikeda, T., 2008, "Photomobile Polymer Materials: Towards Light-Driven Plastic Motors," Angew. Chem., **120**(27), pp. 5064–5066.
[13] Li, Y., Teixeira, Y., Parlato, G., Grace, J., Wang, F., Huey, B. D., and Wang, X., 2022, "Three-Dimensional Thermochromic Liquid Crystal Elastomer Structures With Reversible Shape-Morphing and Color-Changing Capabilities for Soft Robotics," Soft Matter, **18**(36), pp. 6857–6867.
[14] Pang, W., Xu, S., Liu, L., Bo, R., and Zhang, Y., 2023, "Thin-Film-Shaped Flexible Actuators," Adv. Intell. Syst., **5**(8), p. 2300060.

[15] Azoug, A., Vasconcellos, V., Dooling, J., Saed, M., Yakacki, C. M., and Nguyen, T. D., 2016, "Viscoelasticity of the Polydomain-Monodomain Transition in Main-Chain Liquid Crystal Elastomers," Polymer, **98**, pp. 165–171.
[16] Ambulo, C. P., Tasmim, S., Wang, S., Abdelrahman, M. K., Zimmern, P. E., and Ware, T. H., 2020, "Processing Advances in Liquid Crystal Elastomers Provide a Path to Biomedical Applications," J. Appl. Phys., **128**(14), p. 140901.
[17] He, Q., Zheng, Y., Wang, Z., He, X., and Cai, S., 2020, "Anomalous Inflation of a Nematic Balloon," J. Mech. Phys. Solids, **142**, p. 104013.
[18] Tokumoto, H., Zhou, H., Takebe, A., Kamitani, K., Kojio, K., Takahara, A., Bhattacharya, K., and Urayama, K., 2021, "Probing the In-Plane Liquid-Like Behavior of Liquid Crystal Elastomers," Sci. Adv., **7**(25), p. eabe9495.
[19] Modes, C., Warner, M., Van Oosten, C., and Corbett, D., 2010, "Anisotropic Response of Glassy Splay-Bend and Twist Nematic Cantilevers to Light and Heat," Phys. Rev. E, **82**(4), p. 041111.
[20] Korner, K., Kuenstler, A. S., Hayward, R. C., Audoly, B., and Bhattacharya, K., 2020, "A Nonlinear Beam Model of Photomotile Structures," Proc. Natl. Acad. Sci. U. S. A., **117**(18), pp. 9762–9770.
[21] Jin, L., Zeng, Z., and Huo, Y., 2010, "Thermomechanical Modeling of the Thermo-Order–Mechanical Coupling Behaviors in Liquid Crystal Elastomers," J. Mech. Phys. Solids, **58**(11), pp. 1907–1927.
[22] Traugutt, N. A., Volpe, R. H., Bollinger, M. S., Saed, M. O., Torbati, A. H., Yu, K., Dadivanyan, N., and Yakacki, C. M., 2017, "Liquid-Crystal Order During Synthesis Affects Main-Chain Liquid-Crystal Elastomer Behavior," Soft Matter, **13**(39), pp. 7013–7025.
[23] Warner, M., and Terentjev, E. M., 2007, *Liquid Crystal Elastomers*, Oxford University Press, Oxford, UK.
[24] Biggins, J. S., Warner, M., and Bhattacharya, K., 2012, "Elasticity of Polydomain Liquid Crystal Elastomers," J. Mech. Phys. Solids, **60**(4), pp. 573–590.
[25] DeSimone, A., and Teresi, L., 2009, "Elastic Energies for Nematic Elastomers," Phys. Rev. E, **29**(2), pp. 191–204.
[26] DeSimone, A., and Dolzmann, G., 2002, "Macroscopic Response of Nematic Elastomers Via Relaxation of a Class of SO(3)-Invariant Energies," Arch. Ration. Mech. Anal., **161**(3), pp. 181–204.
[27] Yakacki, C., Saed, M., Nair, D., Gong, T., Reed, S., and Bowman, C., 2015, "Tailorable and Programmable Liquid-Crystalline Elastomers Using a Two-Stage Thiol–Acrylate Reaction," RSC Adv., **5**(25), pp. 18997–19001.
[28] Conti, S., DeSimone, A., and Dolzmann, G., 2002, "Semisoft Elasticity and Director Reorientation in Stretched Sheets of Nematic Elastomers," Phys. Rev. E Stat. Nonlin. Soft Matter Phys., **66**(6 Pt 1), p. 061710.
[29] Urayama, K., Kohmon, E., Kojima, M., and Takigawa, T., 2009, "Polydomain-Monodomain Transition of Randomly Disordered Nematic Elastomers With Different Cross-Linking Histories," Macromolecules, **42**(12), pp. 4084–4089.
[30] Bladon, P., Terentjev, E., and Warner, M., 1993, "Transitions and Instabilities in Liquid Crystal Elastomers," Phys. Rev. E, **47**(6), pp. R3838–R3840.
[31] Maier, W., and Saupe, A., 1959, "Eine einfache molekular-statistische Theorie der nematischen kristallinflüssigen Phase. Teil 11," Z. Naturforsch., **14**(10), pp. 882–889.
[32] Corbett, D., and Warner, M., 2006, "Nonlinear Photoresponse of Disordered Elastomers," Phys. Rev. Lett., **96**(23), p. 237802.
[33] Corbett, D., and Warner, M., 2008, "Polarization Dependence of Optically Driven Polydomain Elastomer Mechanics," Phy. Rev. E, **78**(6 Pt 1), p. 061701.
[34] Schätzle, J., Kaufhold, W., and Finkelmann, H., 1989, "Nematic Elastomers: The Influence of External Mechanical Stress on the Liquid-Crystalline Phase Behavior," Die Makromolekulare Chemie, **190**(12), pp. 3269–3284.